

PAPER • OPEN ACCESS

## A vibration compensation optimization method for a mobile atomic gravimeter



To cite this article: Wen-Bin Gong *et al* 2023 *Meas. Sci. Technol.* **34** 055014

View the [article online](#) for updates and enhancements.

### You may also like

- [An atomic gravimeter dynamic measurement method based on Kalman filter](#)  
Chun-Fu Huang, An Li, Fang-Jun Qin et al.
- [Accuracy and stability evaluation of the <sup>85</sup>Rb atom gravimeter WAG-H5-1 at the 2017 International Comparison of Absolute Gravimeters](#)  
Pan-Wei Huang, Biao Tang, Xi Chen et al.
- [Micro-Gal level gravity measurements with cold atom interferometry](#)  
Min-Kang Zhou, , Xiao-Chun Duan et al.

# A vibration compensation optimization method for a mobile atomic gravimeter

Wen-Bin Gong<sup>1</sup> , An Li<sup>1</sup>, Jin-Xiu Ma<sup>1</sup>, Biao Tang<sup>2,\*</sup> and Fang-Jun Qin<sup>1,\*</sup> 

<sup>1</sup> College of Electrical Engineering, Naval University of Engineering, Wuhan 430033, Hubei, People's Republic of China

<sup>2</sup> State Key Laboratory of Magnetic Resonance and Atomic and Molecular Physics, Innovation Academy for Precision Measurement Science and Technology, Chinese Academy of Sciences, Wuhan 430071, People's Republic of China

E-mail: [biaotang@wipm.ac.cn](mailto:biaotang@wipm.ac.cn) and [haig2005@126.com](mailto:haig2005@126.com)

Received 7 November 2022, revised 13 January 2023

Accepted for publication 29 January 2023

Published 17 February 2023



CrossMark

## Abstract

Information on the Earth's gravity provides significant strategic support for economies, defense and security. An atomic gravimeter (AG) realizes highly precise measurements of gravitational acceleration by virtue of atomic interference. Vibration noise is a strong contributor to limitations on the measurement sensitivity and accuracy of an AG. Vibration compensation methods thus enhance the environmental adaptability of an AG since it can facilitate the measurement of gravity when an isolation platform is unavailable. A dynamic compensation filter is here devised for correction of the data output from a seismometer, which expands the bandwidth of the seismometer and lowers the distortion of vibration signals. Additionally, a transfer function estimation is introduced to better reflect the actual vibration of the Raman mirror. Based on a simplified transfer function model, this method can modify the interference fringes of the AG in real time. The experimental results show that the proposed optimization method can attenuate the cosine fitting phase uncertainty of interference fringes by up to 85.91%, and reach an uncertainty of about 76.37  $\mu\text{Gal}$  in a complicated vibration environment. The AG's measurement accuracy is effectively improved by the proposed method. It is verified that the proposed method is effective and adaptable in a complicated noise environment.

Keywords: atomic gravimeter, vibration compensation, dynamic compensation, data processing

(Some figures may appear in colour only in the online journal)

## 1. Introduction

Gravity measurement is a significant aspect in geophysics, geological surveys, and inertial navigation [1, 2]. An atomic gravimeter (AG) is a high-precision absolute gravimeter based on atomic interference. It is capable of continuously measuring

absolute gravitational acceleration, with a measurement accuracy can reach the level of a few microgals [3, 4]. Highly precise gravity measurement has been widely demanded, promoting the development of portable, mobile, and dynamic AGs. For this reason, an AG must be highly adaptable to the environment [5, 6]. Nevertheless, their measurement accuracy and reliability are considerably restricted by vibration noise in complicated environments [7]. In atomic interference measurement, the vibration noise of the Raman mirror is not only the principal contributor to the measurement noise of an AG, but is also a significant constraint on the resolution and sensitivity of gravity measurement. The measurement uncertainty caused by ground vibration may exceed 10  $\mu\text{Gal}$ ,

\* Authors to whom any correspondence should be addressed.



Original content from this work may be used under the terms of the [Creative Commons Attribution 4.0 licence](https://creativecommons.org/licenses/by/4.0/). Any further distribution of this work must maintain attribution to the author(s) and the title of the work, journal citation and DOI.

and even go beyond 10 mGal in a complicated vibration environment. For this reason, it is crucial to inhibit vibration noise.

Presently, vibration noise is commonly inhibited by vibration isolation or compensation [8–11]. A vibration isolation platform is effective in easing the interference caused by vibration on gravity measurement, and helps to achieve good accuracy measurement [12]. However, they are characterized by large size, complex systems, and difficulty in handling. In the process of vibration compensation, the vibration of the Raman mirror is measured, and the fringes are reconstructed after removing the vibration-induced phase shift [7, 13]. Vibration compensation may not be as effective as vibration isolation, but facilitates integrated, compact, and mobile designs of AGs. Therefore, vibration compensation is of great practical significance [14, 15].

Measuring the vibration of the Raman mirror is crucial to vibration compensation. Vibration can be implemented directly or indirectly. In the process of direct measurement, a mirror is taken as a sensitive mass, and its motion is measured by a self-made sensor. This realizes highly accurate compensation, but it is difficult to implement. The devised sensors are characterized by narrow bandwidth, making it impossible to measure absolute gravity in more complicated vibration environments [16, 17]. Indirect measurement relies on utilizing a commercial vibration sensor to measure the motion of the Raman mirror. Nevertheless, it is not easy to estimate the transfer function of the sensor and the Raman mirror. In the process of indirect measurement, the vibration measured by the sensor is used in vibration compensation by simply equaling it to the vibration of the Raman mirror. A low accuracy of compensation therefore results in complicated vibration environments since the transfer function of the sensor and the transfer function from the sensor to the Raman mirror are overlooked. Bidel *et al* [18, 19] constructed a shipboard and airborne absolute gravity measurement system with the Raman mirror placed on an accelerometer, which realized absolute gravity measurement in milligals after vibration compensation in a dynamic environment. In China, shipboard and vehicle-mounted dynamic measurements have been performed by scholars from the Zhejiang University of Technology [20], Naval University of Engineering [21, 22], and Huazhong University of Science and Technology [11]. In their studies, an accelerometer was employed to measure the vibration of a Raman mirror for vibration compensation, leading to highly accurate gravity measurements. In order to measure the actual vibration of the Raman mirror, Xu *et al* [13] adopted commercial inversion software for fast Fourier transform of the waveforms captured by a seismometer, and obtained the frequency spectrum of vibration. The frequency spectrum was modified by the transfer function determined from the measurement and then inverted into the time domain waveform through inverse fast Fourier transform. The inversion of the transfer function was experimented with, revealing an order-of-magnitude improvement after vibration compensation. In this case, the vibration compensation method was nearly half of the effectiveness of the vibration isolation method. However, vibration compensation was more effective

when the external vibration was more dramatic, and capable of compensation for the phase generated by the vibration noise greater than  $4\pi$ .

In vibration compensation for an AG, it is difficult to gather information on the actual vibration of the Raman mirror. First, a high-precision sensor is crucial to vibration measurement. Wen *et al* [23] conducted a controlled experiment, and concluded that a seismometer achieved better compensation than an accelerometer, and could realize a single measurement standard deviation greater than 100 microgals. Due to the limited bandwidth and range (normally less than 50 Hz), the increasing high-frequency components of vibration noise lead to signal distortions in the readings of seismometers, including amplitude attenuation and phase distortion. Thus, the effect of compensation declines. In contrast, the accelerometer was characterized by large bandwidth and good dynamic performance. It was able to realize a measurement standard deviation in milligals under complicated and dynamic conditions, but was still troubled by low resolution and low-frequency drift. Le Gouët *et al* [7] combined a regressive infinite impulse response filter with a non-causal low-pass filter. With a damping for the vibration of above 30 Hz, the compensation by filtering achieved a 25% better vibration inhibition than compensation directly using the data from a seismometer. Moreover, the mechanical transfer function, resulting from different mounting positions for the vibration sensor and the Raman mirror, acted as another major influence on the accuracy of vibration compensation. Wang *et al* [24] proposed a transfer function simplification model, which simplified a transfer function into a gain and delay model. This model presented an effective way to address the difficulty in transfer function estimation and the variation of transfer function with the change of reflector installation method and temperature. It was then applied in the vibration compensation of an optical absolute gravimeter. A high-precision seismometer was also employed to detect the vibration signals. Following this, a correlation analysis or golden section method was used to search two coefficients, that is, gain and relay. As a result, the trajectory signals of falling objects were modified to provide favorable compensation. Yao *et al* [25] applied a simplified transfer function to the vibration compensation of an AG for the first time, which delivered good compensation in a tranquil testing environment. However, this was not verified in a complicated vibration environment.

To improve the vibration compensation of an AG in a complicated vibration environment, a vibration compensation optimization method is here proposed for mobile AGs considering dynamic characteristic compensation of seismometers. As aforementioned, being characterized by low noise and high sensitivity, a seismometer is selected for vibration measurement. A dynamic compensation filter is therefore devised to cope with the narrow bandwidth of a seismometer. It is used to correct a seismometer's output data, which effectively increases its bandwidth and reduces vibration signal distortions. Furthermore, a simplified transfer function model is employed and optimized by an improved sparrow search algorithm to determine the optimal gain and delay.

The transfer function is fast-estimated to better reflect the real vibration of the Raman mirror and real-time correction of the interference fringes of the AG. An experiment is carried out to assess the interference fringe fitting phase uncertainty of an AG and the Allen deviation of gravity measurements. The effect of the proposed method on vibration compensation is analyzed to facilitate the application of an AG in a complicated vibration environment.

## 2. Principles

### 2.1. Vibration compensation for an AG

An AG is used to measure absolute gravity utilizing the basic principle of the wave interference of atomic matter under the joint effect of Raman lasers and cold atoms. During its free fall, a sample of cold atoms is triggered by a  $\pi/2-\pi-\pi/2$  Raman laser pulse to be split, reflected and combined, which results in matter wave interference. Following this, normalized detection is conducted to capture the fluorescence signal of the atoms and to determine the atomic transition probability  $P$ . The interference fringes satisfy  $P = P_0 + C/2\cos(\Delta\Phi)$ , where  $P_0$ ,  $C$  and  $\Delta\Phi$  stand for the probability bias, contrast and phase of the atomic interference fringes, respectively. Because of the Doppler shift, the frequency of the Raman laser must be scanned linearly to guarantee the atomic resonance with the Raman laser in the falling process. The phase,  $\Delta\Phi$ , is defined by

$$\Delta\Phi = (k_{\text{eff}}g - 2\pi\alpha)T^2, \quad (1)$$

where  $k_{\text{eff}}$  is the effective wave vector,  $\alpha$  is the chirp rate of the Raman laser's frequency, and  $T$  is the time interval of Raman pulses. The interference fringes are eventually fitted by a least-squares method to determine the gravity.

In practical measurement, the actual phase of an AG contains a phase shift,  $\Delta\Phi_{\text{vib}}$ , caused by the vibration of the Raman mirror as follows:

$$\Delta\Phi = (k_{\text{eff}}g - 2\pi\alpha)T^2 + \Delta\Phi_{\text{vib}}. \quad (2)$$

A vibration sensor can be used to measure the vibration of the Raman mirror. The value  $\Delta\Phi_{\text{vib}}$  can be determined by equation (3):

$$\Delta\Phi_{\text{vib}} = k_{\text{eff}} \int_0^{2T+4\tau} g_s(t)v(t)dt, \quad (3)$$

where  $g_s(t)$  is the velocity sensitivity function of the gravimeter and  $v(t)$  is the vertical vibration velocity of the Raman mirror. The sensitivity function,  $g_s(t)$ , is given by equation (4) [26]:

$$g_s(t) = \begin{cases} 0 & t < -T - 2\tau \\ \sin\Omega_R(T+t) & -T - 2\tau \leq t < -T - \tau \\ -1 & -T - \tau \leq t < -\tau \\ \sin\Omega_R t & \tau \leq t < T + \tau \\ -\sin\Omega_R(T-t) & T + \tau \leq t < T + 2\tau \\ 0 & t \geq T + 2\tau \end{cases}, \quad (4)$$

where  $\Omega_R$  is the Rabi frequency and  $\tau$  is the length of a finite Raman pulse. As a result, the calculated phase shift for the vibration of the Raman mirror is removed. After compensation, a phase transition probability curve is obtained for the reconstruction of fringes to restore the atomic interference fringes. The actual gravitational acceleration is then calculated. The compensation process is shown in figure 1.

### 2.2. Dynamic compensation of seismometer

Dynamic error is caused by hysteresis in the response of a measurement system to a change of an input signal, or caused by different attenuation-gain proportions of the frequencies in the input signal that pass through a measurement system. When measuring vibration with a seismometer, the measured signal is sampled after passing through the seismometer; due to the poor dynamic characteristics of the seismometer, dynamic errors are generated; thus, a dynamic compensation system needs to be built to compensate for this and to improve the measurement accuracy [27]. The framework of a dynamic compensation system for a seismometer is presented in figure 2.

In figure 2,  $v(t)$  is the actual measured signal and  $v_{\text{mea}}(t)$  is the signal measured by the seismometer. The poor dynamicity of the seismometer causes the difference between  $v_{\text{mea}}(t)$  and  $v(t)$ , resulting in the aforementioned dynamic error. The seismometer system is denoted by  $G(z)$ , and the dynamic compensation parameters form a system  $C(z)$ . The output signal of the seismometer,  $v_{\text{mea}}(t)$ , becomes  $v_{\text{com}}(t)$  after compensation. The output signal  $v_{\text{com}}(t)$  is closer to the measured signal  $v(t)$ . Put simply, the output after compensation  $v_{\text{com}}(t)$  replaces the seismometer output  $v_{\text{mea}}(t)$ , as illustrated in figure 2:

$$v_{\text{mea}}(t) = G(z)v(t), \quad (5)$$

$$v_{\text{com}}(t) = C(z)v_{\text{mea}}(t). \quad (6)$$

Dynamic compensation intends to expand the working frequency band of the seismometer, to cover the main frequency components of the measured signal fully or as much as possible. It is realized by serially connecting a compensation unit to the output end. The unit often contains a compensation filter that changes the amplitude and frequency components of the seismometer's output signal [28]. In other words, it increases the original system bandwidth and inhibits the signal at the resonance frequency.

The dynamic compensation system  $C(z)$  is determined by  $v_{\text{mea}}(t)$  and  $v_{\text{com}}(t)$  with the differential equations as follows:

$$A(z^{-1})v_{\text{mea}}(t) = B(z^{-1})v_{\text{com}}(t), \quad (7)$$

$$C(z) = \frac{A(z^{-1})}{B(z^{-1})} = \frac{a_0 + a_1z^{-1} + a_2z^{-2} + \dots + a_nz^{-n}}{1 + b_1z^{-1} + b_2z^{-2} + \dots + b_nz^{-n}}, \quad (8)$$

where  $a_0, a_1, \dots, a_n$  and  $b_1, b_2, \dots, b_n$  represent the coefficients of the compensation system, and  $n$  stands for the order of the

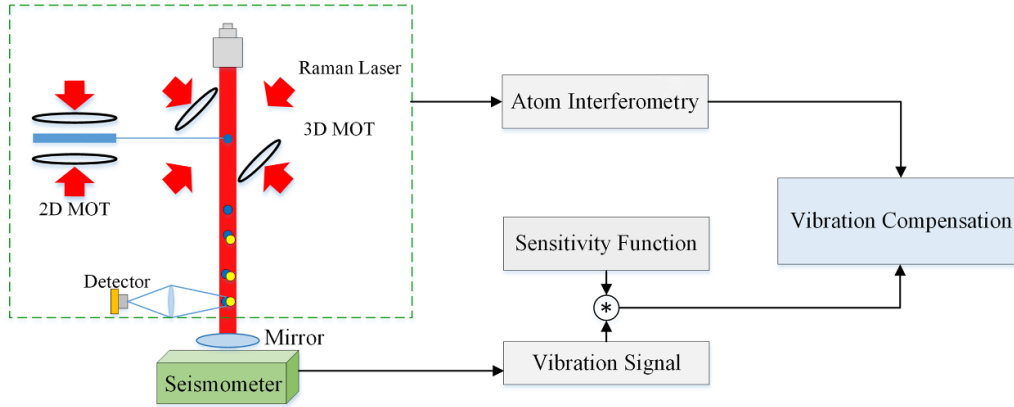


Figure 1. Vibration compensation for an atomic gravimeter.

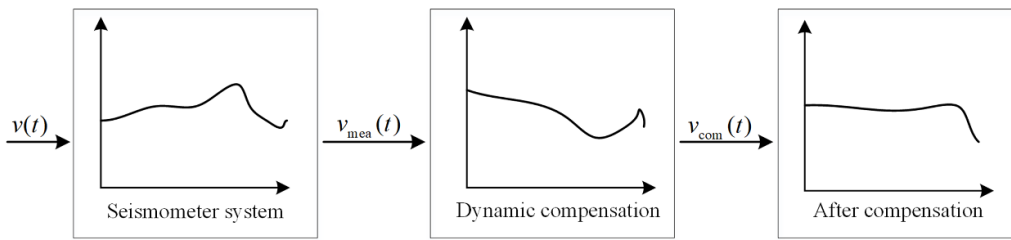


Figure 2. Framework of a dynamic compensation model for a seismometer.

compensation system. Ideally, there is  $C(z)G(z) = 1$ , implying that the signal is not distorted after dynamic compensation. Nevertheless, the signal is unstable according to the Nyquist criterion. A non-ideal compensation unit is utilized for compensation to reduce the error of dynamic measurement, and make the objective function  $J = \sum_{k=0}^{N-1} [v(k) - v_{com}(k)]^2 \rightarrow \min$ , where  $v(k)$  is the step signal and  $v_{com}(k)$  is the data of the test signal through the bandwidth compensation system. In this way, the seismometer can meet the requirements of the application.

### 2.3. Transfer function estimation

The actual vibration of a Raman mirror is measured, and then used to calculate the phase shift driven by such vibration. This provides the compensation for the measurement of an AG. Nevertheless, the output signal of the seismometer is not equal to the actual vibration of the Raman mirror; their relationship is shown in figure 3. In the figure,  $v_0$  denotes the ground motion,  $v_{Rm}$  indicates the motion of the Raman mirror,  $v_{mea}$  is the output velocity of the seismometer,  $G_a$  represents the transfer function from the ground motion to the reference prism motion,  $G_b$  stands for the transfer function from the ground motion  $v_0$  to the input of the seismometer, and  $G_c$  is the transfer function of the seismometer.

The transfer function between the actual vibration velocity of the Raman mirror and the output signal of the seismometer satisfies

$$v_{Rm} = \frac{v_{mea}}{G_c} \frac{G_a}{G_b} = v_{mea} H_N. \quad (9)$$

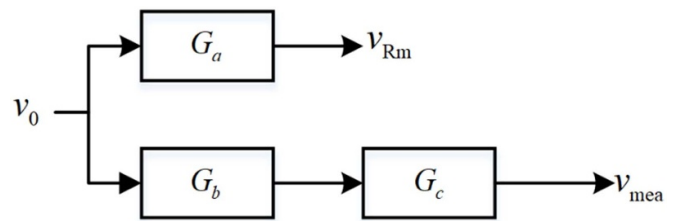


Figure 3. Relationship between the output of the seismometer and the vibration of the Raman mirror.

Vibration compensation can be implemented after solving the transfer function  $H_N$ , as it is affected by the accuracy of this transfer function. Among them,  $G_c$  is provided by the seismometer's manufacturer or measured at the site. Nevertheless, drift may occur at different times or situations. In the field or in other complicated environments, the actual transfer function may be different from the stated measurement transfer function because of dramatically varying ambient temperature or humidity. Consequently, the seismometer must be periodically calibrated. Moreover,  $G_a/G_b$  also vary with some factors such as the distance from the seismometer to the Raman mirror and how they are attached. It is difficult to directly measure  $G_a/G_b$ , which is approximately 1 only if the distance is short and the attachment is secure. As a consequence, the transfer function  $H_N$  is difficult to directly measure and often varies in application.

In a practical system, delay is an inevitable problem for machines and circuits no matter what type of sensor is used



to measure the motion of the Raman mirror. Additionally, a sensor's sensitivity may be affected by estimation error to drift with changes of time and temperature. However, the measurement environment will not change significantly in a single gravity-measurement task: in this case, a delay coefficient,  $\gamma$ , and a gain coefficient,  $A$ , can be combined into a simplified transfer function model to estimate  $H_N$  [29, 30]. It is believed that the values of these two coefficients remain unchanged during the current measurement process [24]. The actual motion of a Raman mirror can be expressed as

$$v_{\text{Rm}}(t) = A \cdot v_{\text{mea}}(t + \gamma). \quad (10)$$

Based on the principle of atomic interference gravity measurement, the relationship between atomic transition probability and interference phase forms a trigonometric function. As a result, the parameters of the transfer function can be determined by assessing the reconstruction of the interference fringes and by fitting of a cosine waveform. This is essentially a problem of optimization. The residual error of fitting is represented by  $f(A, \gamma)$ , where  $(A, \gamma)$  belongs to the set  $K$ . The model for this problem can be expressed as

$$\begin{aligned} &\min f(x), \\ &s.t. x \in K \end{aligned} \quad (11)$$

Over several periods of atomic interference, the chirp rate is scanned to determine the atomic interference fringes. The set  $K$  is traversed to minimize the residual error in the fitting of the compensated interference fringes and cosine curve, which realizes the best fit. It is believed that the gain coefficient,  $A_{\text{opt}}$ , and the time delay,  $\gamma_{\text{opt}}$ , are optimal at this time. In this way, the transfer function is estimated. After that, the estimated transfer function is used to restore the vibration of the Raman mirror. With equation (3), the phase change caused by the vibration noise in each atomic interference period is determined to obtain the atomic interference fringes after removing the influence of vibration noise.

### 3. Experiment

#### 3.1. Apparatus

A self-made, compact and mobile AG was used in this experiment. It consisted of vacuum, optical and control systems, with the indicators for its performance detailed in [31]. The interference time interval of this system was  $T = 71$  ms. The measurement was conducted in the form of fringe scanning. During measurement, the Raman laser vector  $k_{\text{eff}}$  remained unchanged, but the scan frequency  $\alpha$  increased linearly. Each set of data contained 20 atomic interferences, which were fitted into an interference fringe.

A low-noise and low-frequency broadband seismometer (CMG-3V, Guralp Systems Ltd) was used to measure motion. Its effective bandwidth was 0.0027–50 Hz. Its noise level of 0.01–10 Hz was lower than  $4 \times 10^{-9} (\text{m s}^{-2})/\sqrt{\text{Hz}}$ . Its

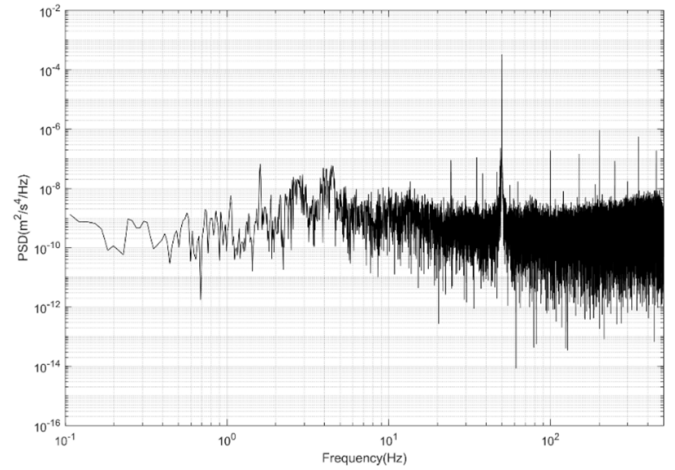


**Figure 4.** Power spectrum density of ground vibration noise at the laboratory.

sensitivity was around  $2000 \text{ V m}^{-1} \text{ s}^{-1}$ . A temperature-compensated suspension spring was adopted to considerably lower the temperature dependence and reduce the low-frequency drift. This seismometer has been widely applied in active vibration isolation systems [32] and in the AG at Stanford University [33, 34].

#### 3.2. Vibration noise

The experiment was conducted in a fourth-floor laboratory. The laboratory is located in an office area but is surrounded by traffic, buildings, and large mechanical vibration sources. During the experiment, vibration isolation was not adopted. The power spectrum density (PSD) of ground vibration acceleration at the laboratory is shown in figure 4.

In the PSD diagram for vibration noise at the laboratory, the 0.1–0.5 Hz noise was mainly caused by microseisms of the Earth, the noise around 2 Hz originated from the natural vibration of the building, and the noise found at 10–20 Hz was attributed to human activities. The noise of higher frequencies resulted from the vibration of instruments in operation. There was a large characteristic peak at a frequency of around 50 Hz [35]. These noises were coupled into the inertial noise for the AG.

To further assess the influence of vibration on the AG at the laboratory, the relationship between the vibration acceleration transfer function and the AG transfer function can be expressed as

$$|H_a(\omega)|^2 = \frac{k_{\text{eff}}^2}{\omega^4} |H_\phi(\omega)|^2, \quad (12)$$

where  $H_\phi(\omega)$  is the transfer function between the AG's interference phase and the Raman laser's modulation phase. It is given by equation (13):

$$\begin{aligned} H_\phi(\omega) = & -\frac{4i\Omega_R\omega}{\omega^2 - \Omega_R^2} \sin\left(\omega \frac{T+2\tau}{2}\right) \left[ \cos\left(\omega \frac{T+2\tau}{2}\right) \right. \\ & \left. + \frac{\Omega_R}{\omega} \times \sin\left(\omega \frac{T}{2}\right) \right]. \end{aligned} \quad (13)$$

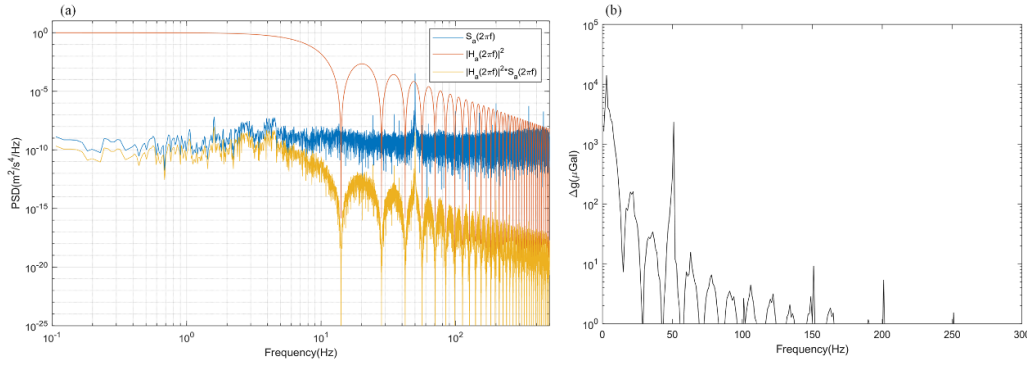


**Figure 5.** Influence of vibration noise on a gravimeter. (a) The blue line indicates the power spectrum density (PSD) of vibration noise at the laboratory, the red line is the normalized transfer function with  $T = 71$  ms, and the orange line represents the resultant PSD of vibration noise and transfer function. (b) Integration analysis of vibration noise by frequency band.

The contribution of vibration to the gravimeter can be obtained by integration after convolution of the PSD  $S_a(\omega)$  and the transfer function of vibration acceleration:

$$(\sigma_g^{\text{rms}})^2 = \int_0^{\infty} |H_a(\omega)|^2 S_a(\omega) d\omega. \quad (14)$$

In figure 5(a), the red line indicates the normalized transfer function of  $T = 71$  ms, the blue line represents the PSD of ground vibration noise, and the orange line stands for their convolution. This helps more vividly analyze the influence of vibration on the gravimeter. The orange line is integrated to determine the phase caused by vibration noise. The phase shift resulting from the ground vibration noise at the laboratory is  $3.9 \pi$  rad. After integration for each frequency band, the contribution of the vibration of each frequency band to the phase of the gravimeter can be determined, as shown in figure 5(b). The phase fluctuates dramatically in the 0.1–100 Hz frequency band, and the influence of the frequency band below 200 Hz exceeds  $1 \mu\text{Gal}$ .

While assessing the influence of vibration noise on the AG, attention should be paid to the intensity of the noises of different frequencies at the place of measurement. Moreover, the influences of the different frequency noises on the AG should be also taken into account. In a complicated vibration environment, noises are mainly caused by human activities and mechanical vibrations, and are of relatively higher frequency, in particular around 25 Hz and 50 Hz. For this reason, noise in the range of 0.1–200 Hz must be carefully addressed.

### 3.3. Procedure

The experiment was carried out in four steps with the technical route as shown in figure 6, including measurement by an AG and vibration signal acquisition, vibration signal correction, transfer function estimation and vibration compensation. The specific procedure of this experiment is described as follows.

**Step 1:** Undertake measurement with an AG with the simultaneous collection of data from a seismometer. In this system, time synchronization is dependent on an atomic clock. It was controlled to label and begin the collection of vibration data at the time of the first  $\pi/2$  Raman interference. Considering the delay of data, it was set to initiate the collection 0.1 s ahead of the first  $\pi/2$  Raman interference, and to end it 0.1 s after the last  $\pi/2$  Raman interference. This was intended for the subsequent correction of vibration data.

**Step 2:** Correction of vibration signals. The bandwidth of the vibration measurement device was less than 50 Hz. This must be improved since it is not possible to satisfy the requirements for high-frequency vibration measurement in a complicated environment. Dynamic compensation was therefore performed for the seismometer to increase the measurement bandwidth and gather more real vibration signals. For this reason, a compensation filter was devised. With an improved particle swarm optimization algorithm, the parameters of the compensation filter were determined after multiple iterations. The transfer function for the compensation filter,  $C(z)$ , is as follows:

$$C(z) = \frac{5.137 + 16.64z - 2.11z^2 - 13.29z^3 - 21.99z^4 - 2.48z^5 + 9.16z^6 + 9.54z^7 - 0.37z^8}{1 - 0.48z - 0.07z^2 - 0.45z^3 - 0.18z^4 + -0.47z^5 + 0.67z^6 + 0.02z^7 + 0.19z^8}. \quad (15)$$

The determined parameters were used to construct a compensation filter model and draft a Bode diagram before and after the compensation for the seismometer, as shown in

figure 7. Evidently, the effective bandwidth of the transfer function was increased from 50 Hz to 150 Hz ( $-3$  dB) after the compensation. After being tripled, the bandwidth approached

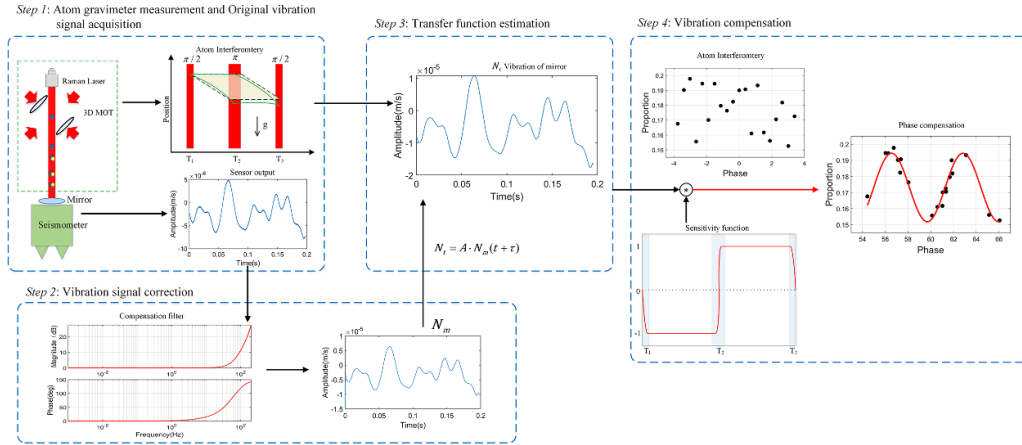


Figure 6. Technical route of vibration compensation optimization.

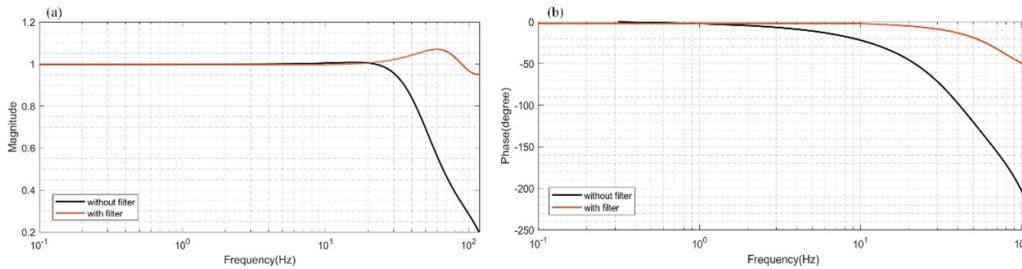


Figure 7. Bode diagram before and after the compensation for the seismometer.

a normal value. Additionally, the phase delay was also alleviated. After the compensation, the transfer function of the seismometer was closer to the time delay.

**Step 3:** Use corrected vibration signals to estimate the transfer function and determine the coefficients including gain and delay. The sparrow search algorithm is a novel intelligent swarm optimization algorithm. It is greatly advantageous in terms of convergence, stability and robustness. Nevertheless, it is also troubled by premature convergence. As an improved version, the chaotic sparrow search algorithm (CSSA) was adopted with cosine chaotic mapping and the genetic operator mutation operation, to improve the global search capability of the algorithm [36].

**Step 4:** Use the gain coefficient and delay obtained in Step 3 with the simplified transfer function model of equation (10) to restore the vibration of the Raman mirror. The vibration-induced phase shift is then determined by equation (3). Vibration compensation is completed after removing the phase shift.

#### 4. Results

In order to reduce the randomness of single measurements, the experimental data were selected in 20 interference periods for the transfer function estimation. After the data were optimized with the CSSA, 20 optimal gains and delays were determined, as given in figure 8. The average value of these gains

was approximately 1.469 with a standard deviation of 0.037. The average value of these delays was 1.78 ms with a standard deviation of 0.095. Considering their centralized distribution and low standard deviation, it was believed that the average values could reflect the actual performance of the system. Therefore, the average values were taken for gain coefficient and delay.

Figure 9 presents the interference fringes after vibration compensation through the proposed optimization. The phase uncertainty of cosine fitting was 62 mrad, and the corresponding gravity measurement uncertainty was 76.37  $\mu$ Gal. The proposed optimization realized the favorable restoration of effective interference fringes. However, the data after compensation still contained noises introduced by other sources into the system.

A controlled experiment was carried out to prove the superiority of the optimized vibration compensation method and to determine the role of the seismometer's dynamic characteristic compensation and transfer function estimation in the optimized method. The compensation with the proposed method was compared with three other methods of compensation. Method 1 is to use the seismometer measurement data for direct compensation; that is, without steps 2 and 3. Method 2 is to use bandwidth seismometer compensation but without transfer function estimation; that is, including Step 2 but not Step 3. Method 3 is to use transfer function estimation but without bandwidth seismometer compensation; that



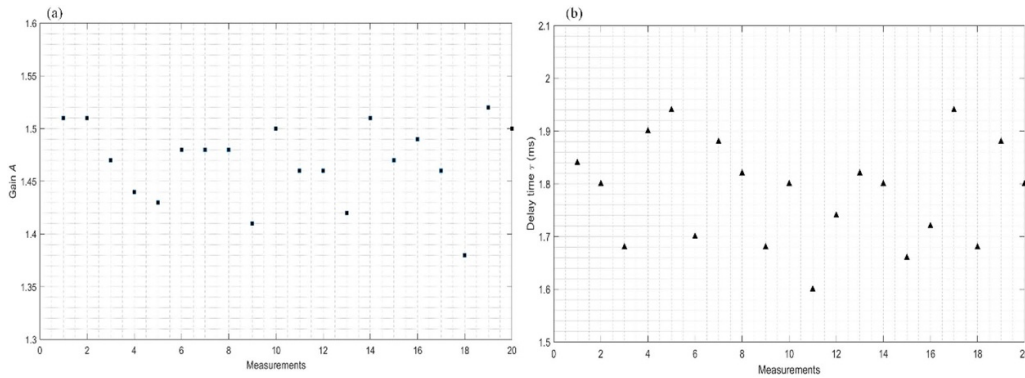


**Figure 8.** Gains and delays obtained from 20 measurements. (a) Gains, (b) delays.

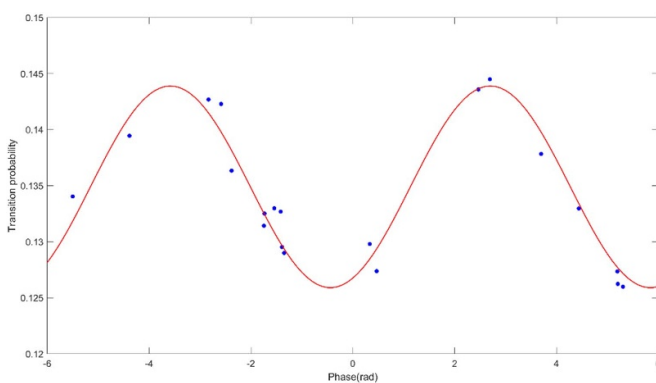


**Figure 9.** Interference fringes after the proposed compensation. The blue points indicate the experimental data from 20 points, and the red line is the cosine function fitting curve.

is, carrying out Step 3 but without Step 2; Yao *et al* used this method in [25]. The effects of the various compensation methods are shown in figure 10. The original measurements without compensation are given in figure 10(a). It is evident that the atomic interference fringes have been entirely flooded by excessive vibration noise. The fringe fitting failed, making it impossible to measure gravity. In figure 10(b), the results after compensating with Method 1 reveal the poor effect. The measured vibration signals are severely distorted because of too much vibration noise and the narrow bandwidth of the seismometer. The phase uncertainty of cosine fitting is 439.57 mrad, and the uncertainty of gravity measurement is 541.95  $\mu\text{Gal}$ . In order to verify the constraint of the seismometer's bandwidth on vibration compensation, Method 2 was employed for vibration compensation. The results are illustrated in figure 10(c). It is revealed that the fringe fitting is improved after correcting the data from the seismometer. The phase uncertainty of cosine fitting is 230.5 mrad, while the uncertainty of gravity measurement is 283.91  $\mu\text{Gal}$ . Since transfer function estimation was also shown to play a significant role in vibration compensation, it is implemented in Method 3. The results obtained after estimation were then used for vibration compensation. The compensated interference fringes are given in figure 10(d). The phase uncertainty

of cosine fitting is 160.34 mrad, and the uncertainty of gravity measurement is 197.49  $\mu\text{Gal}$ . In other words, transfer function estimation can also improve the accuracy of vibration compensation.

Allan deviation analysis was performed with the gravity deviation after compensation to further explore the influence of the proposed method on gravity measurement. The results are given in figure 11. As revealed in the figure, the gravity measurement resolution of methods 1, 2 and 3 are 367  $\mu\text{Gal}$ , 221  $\mu\text{Gal}$  and 163  $\mu\text{Gal}$ , respectively, after the 96 s integration (without tidal effect being compensated for). However, the gravity measurement resolution of the proposed method reaches 106  $\mu\text{Gal}$  at 96 s. The proposed method has an Allan deviation 71.12% lower than the direct vibration compensation. Therefore, the optimized vibration compensation method can deliver a satisfying gravity measurement in a severely noisy environment, as well as meet requirements for measurement in the field.

In table 1, the experimental results of the different compensation methods are given for a clear analysis. The comparison with Method 1 (direct compensation) can reveal how much the performance is improved. After correcting the data from the seismometer with the compensation filter devised in this paper, the uncertainty of measurement with vibration compensation for the AG was reduced from 541.95  $\mu\text{Gal}$  to 283.91  $\mu\text{Gal}$ . Therefore, the effect of compensation was improved by 47.61%. The resolution of gravity measurement after the 96 s integration increased from 367  $\mu\text{Gal}$  to 221  $\mu\text{Gal}$ , which was a 39.78% improvement. This implies that the compensation filter expanded the bandwidth of the seismometer and satisfactorily restored the vibration signals. Moreover, transfer function estimation helped lower the uncertainty of measurement with vibration compensation for the AG from 541.95  $\mu\text{Gal}$  to 197.49  $\mu\text{Gal}$ . The effect of compensation was improved by 63.56%. The resolution of gravity measurement after the 96 s integration increased from 367  $\mu\text{Gal}$  to 163  $\mu\text{Gal}$ , which was a 55.59% improvement. Transfer function estimation proved essential in the process. After applying the proposed optimization algorithm, an optimal vibration compensation was achieved. Effectively, the uncertainty of measurement could be further lowered to 76.37  $\mu\text{Gal}$ , and

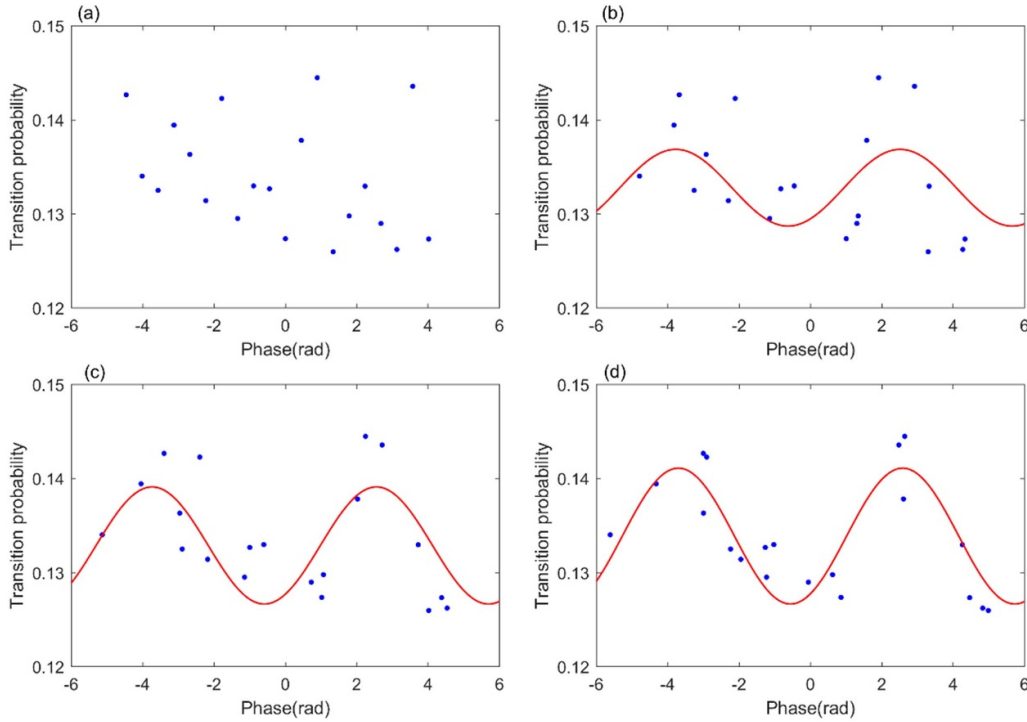


Figure 10. Atomic interference fringes. (a) Uncompensated fringes, (b) Method 1, (c) Method 2, (d) Method 3.

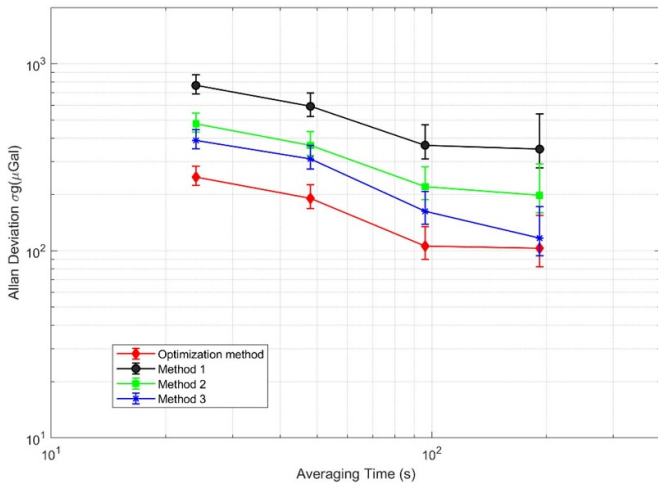


Figure 11. Comparison of gravity measurements after vibration compensation in terms of Allan deviation.

the resolution of the gravity measurement after the 96 s integration reached 106  $\mu\text{Gal}$ . The effect was therefore improved by 85.91% and 71.12%, respectively, compared with the direct vibration compensation.

### 5. Discussion

Vibration compensation can effectively inhibit vibration noise and enhance the accuracy of gravitational acceleration measurement, especially in a complicated vibration environment. However, the effect of compensation is limited to the vibration measurement of the Raman mirror. Furthermore, atomic

Table 1. Experimental results.

	Uncertainty ( $\mu\text{Gal}$ )	Improved (%)	Measurement resolution ( $\mu\text{Gal}$ @ 96s)	Improved (%)
Method 1	541.95	—	367	—
Method 2	283.91	47.61	221	39.78
Method 3	197.49	63.56	163	55.59
Optimization method	<b>76.37</b>	<b>85.91</b>	<b>106</b>	<b>71.12</b>

interference gravity measurement is exposed to a variety of noise sources including vibration, Raman laser phase and light intensity.

Vibration compensation therefore presently encounters two issues. One is to solve the motion of the Raman mirror based on the output of a sensor; that is, by solving the transfer function. The other is to identify and correct the change of transfer function promptly. The transfer function estimation can improve the vibration compensation accuracy of the AG. In our Method 3, only the transfer function is estimated, and the uncertainty in a single measurement of AG vibration compensation is 197.49  $\mu\text{Gal}$ . However, due to the narrow bandwidth of the seismometer, it is impossible to truly measure the vibration signal under complex environments. The proposed seismometer dynamic compensation filter in this paper can effectively improve the problem of insufficient measurement bandwidth, boost the transfer function gain of the seismometer after bandwidth compensation close to 1, ensure the phase is linear, more in line with the effective conditions of the simple transfer function model, reduce the error caused by the non-equivalence

between the actual transfer function and the simplified model, and increase the uncertainty of the single measurement of the AG vibration compensation to 76.37  $\mu\text{Gal}$ . As a result, it is 61.33% higher than Method 3.

After comparison with existing procedures for vibration compensation, the proposed method is proved to be highly effective in improving the solution accuracy of the transfer function and solving the drift of the transfer function. In applications having lower requirements for accuracy, the transfer function can be reasonably simplified to achieve a balance between accuracy and operability.

The accuracy of vibration compensation can be further improved after performing dynamic compensation for a seismometer. In other words, a compensation filter expands the bandwidth of the transfer function to practically restore the vibration signals. This can effectively reduce the distortion of vibration signals and make the transfer function closer to the simplified model. Nevertheless, such a dynamic compensation system fails to fully correct the amplitude attenuation because of the intrinsically narrow bandwidth of seismometers, making it impossible to perfectly restore high-frequency vibration noise.

## 6. Conclusions

A vibration compensation optimization method for a mobile AG was proposed in this paper. It was combined with dynamic characteristic compensation of a seismometer to resolve the poor vibration compensation effect for AGs in complicated environments. The proposed method can better restore the real vibration of the Raman mirror through dynamic characteristic compensation of the seismometer and transfer function estimation. It achieves better compensation, especially in a complicated vibration environment containing high-frequency vibration. It remains effective even if the vibration-induced phase shift reaches  $3.9\pi$  rad. In an experiment for vibration compensation in a complicated vibration environment, the proposed method was compared with direct compensation using the data from the seismometer. As revealed, it realizes dramatic attenuation of the cosine fitting phase uncertainty for the interference fringes of the AG. The maximum attenuation reaches 85.91%. In addition, the sensitivity of measurement is improved from 541.95  $\mu\text{Gal}$  to 76.37  $\mu\text{Gal}$ . The Allan deviation of the gravity calculated with the corrected interference fringes decreases by 71.12%. Thus, the proposed method is proven to be effective and advanced. The transfer function may vary with the environment, but the proposed method is strongly adaptive. Therefore, it can reasonably estimate the practical transfer function of a structure regardless of the changing environment of measurement, to achieve the best correction of atomic interference fringes, anytime anywhere.

## Data availability statement

The data generated and/or analyzed during the current study are not publicly available for legal/ethical reasons but

are available from the corresponding author on reasonable request.

## Acknowledgments

We thank Dr Ming-Ting Li and Wu Liu for their help in the experiment. This research was supported by the National Natural Science Foundation of China under Grants (Grant No. 42274013).

## ORCID iDs

Wen-Bin Gong  <https://orcid.org/0000-0001-8424-9409>

Fang-Jun Qin  <https://orcid.org/0000-0002-6777-2713>

## References

- [1] Stray B *et al* 2022 Quantum sensing for gravity cartography *Nature* **602** 590–4
- [2] Antoni-Micollier L, Carbone D, Ménoret V, Lautier-Gaud J, King T, Greco F, Messina A, Contrafatto D and Desruelle B 2022 Detecting volcano-related underground mass changes with a quantum gravimeter *Geophys. Res. Lett.* **49** e2022GL097814
- [3] Janvier C, Menoret V, Desruelle B, Merlet S, Landragin A and Dos Santos F P 2022 Compact differential gravimeter at the quantum projection-noise limit *Phys. Rev. A* **105** 022801
- [4] Huang P W, Tang B, Chen X, Zhong J Q, Xiong Z Y, Zhou L, Wang J and Zhan M S 2019 Accuracy and stability evaluation of the 85Rb atom gravimeter WAG-H5-1 at the 2017 international comparison of absolute gravimeters *Metrologia* **56** 7
- [5] Zhang J Y, Chen L L, Cheng Y, Luo Q, Shu Y B, Duan X C, Zhou M K and Hu Z K 2020 Movable precision gravimeters based on cold atom interferometry *Chin. Phys. B* **29** 88–96
- [6] Wu X J, Pagel Z, Malek B S, Nguyen T H, Zi F, Scheirer D S and Muller H 2019 Gravity surveys using a mobile atom interferometer *Sci. Adv.* **5** eaax0800
- [7] Le Gouët J, Mehlstäubler T E, Kim J, Merlet S, Clairon A, Landragin A and Pereira Dos Santos F 2008 Limits to the sensitivity of a low noise compact atomic gravimeter *Appl. Phys. B* **92** 133–44
- [8] Gong W B, Li A, Huang C F, Che H, Feng C X and Qin F J 2022 Effects and prospects of the vibration isolation methods for an atomic interference gravimeter *Sensors* **22** 583
- [9] Zhou M K, Xiong X, Chen L L, Cui J F, Duan X C and Hu Z K 2015 Note: a three-dimension active vibration isolator for precision atom gravimeters *Rev. Sci. Instrum.* **86** 046108
- [10] Zhang J Y, Xu W J, Sun S D, Shu Y B, Luo Q, Cheng Y, Hu Z K and Zhou M K 2021 A car-based portable atom gravimeter and its application in field gravity survey *AIP Adv.* **11** 115223
- [11] Guo J, Ma S, Zhou C, Liu J, Wang B, Pan D and Mao H 2022 Vibration compensation for a vehicle-mounted atom gravimeter *IEEE Sens. J.* **22** 12939–46
- [12] Zhou Y, Luo D Y, Wu B, Cheng B and Lin Q 2020 Active vibration isolation system based on the LADRC algorithm for atom interferometry *Appl. Opt.* **59** 3487–93
- [13] Xu A, Kong D, Fu Z, Wang Z and Lin Q 2019 Vibration compensation of an atom gravimeter *Chin. Opt. Lett.* **17** 070201
- [14] Menoret V, Vermeulen P, Le Moigne N, Bonvalot S, Bouyer P, Landragin A and Desruelle B 2018 Gravity measurements

- below 10(−9) g with a transportable absolute quantum gravimeter *Sci. Rep.* **8** 12300
- [15] Cheng B et al 2022 The research on the experiment of dynamic absolute gravity measurement based on cold atom gravimeter *Acta Phys. Sin.* **71** 026701
- [16] Richardson L L 2019 Inertial noise post-correction in atom interferometers measuring the local gravitational acceleration *Fakultät für Mathematik und Physik Gottfried Wilhelm Leibniz Universität Hannover, Hanover, Lower Saxony*
- [17] Richardson L L et al 2020 Optomechanical resonator-enhanced atom interferometry *Commun. Phys.* **3** 208
- [18] Bidet Y, Zahzam N, Blanchard C, Bonnini A, Cadoret M, Bresson A, Rouxel D and Lequentrec-Lalancette M F 2018 Absolute marine gravimetry with matter-wave interferometry *Nat. Commun.* **9** 627
- [19] Bidet Y, Zahzam N, Bresson A, Blanchard C, Cadoret M, Olesen A V and Forsberg R 2020 Absolute airborne gravimetry with a cold atom sensor *J. Geod.* **94** 20
- [20] Cheng B et al 2021 Absolute gravity measurement based on atomic gravimeter under mooring state of a ship *Acta Phys. Sin.* **70** 040304
- [21] Che H et al 2022 Ship-borne dynamic absolute gravity measurement based on cold atom gravimeter *Acta Phys. Sin.* **71** 148–56
- [22] Huang C-F, Li A, Qin F-J, Fang J and Chen X 2023 An atomic gravimeter dynamic measurement method based on Kalman filter *Meas. Sci. Technol.* **34** 015013
- [23] Wen Y, Wu K and Wang L 2022 Analysis of vibration correction performance of vibration sensor for absolute gravity measurement *Acta Phys. Sin.* **71** 049101
- [24] Wang G, Hu H, Wu K and Wang L J 2017 Correction of vibration for classical free-fall gravimeters with correlation-analysis *Meas. Sci. Technol.* **28** 035001
- [25] Yao J, Zhuang W, Feng J, Wang Q, Zhao Y, Wang S, Wu S and Li T 2022 A coefficient searching based vibration correction method *Acta Phys. Sin.* **71** 407–23
- [26] Cheinet P, Canuel B, Santos F P D, Gauguier A, Yver-Leduc F and Landragin A 2008 Measurement of the sensitivity function in a time-domain atomic interferometer *IEEE Trans. Instrum. Meas.* **57** 1141–8
- [27] Wang X, Han T, Zhang E, Zhang Y, Liu X and Gong Y 2017 Dynamic compensation of piezoresistive pressure sensors based on fireworks algorithm *Acta Armamentarii* **38** 2226–33
- [28] Pan C, Zhang R, Luo H and Shen H 2018 Target-based algorithm for baseline correction of inconsistent vibration signals *J. Vib. Control* **24** 2562–75
- [29] Wen Y, Wu K and Wang L 2022 Vibration correction system towards dynamic absolute gravimetry *IEEE Trans. Instrum. Meas.* **71** 1–9
- [30] Wen Y, Wu K, Guo M Y and Wang L J 2021 An optimized vibration correction method for absolute gravimetry *IEEE Trans. Instrum. Meas.* **70** 1–7
- [31] Fang J, Hu J G, Chen X, Zhu H R, Zhou L, Zhong J Q, Wang J and Zhan M S 2018 Realization of a compact one-seed laser system for atom interferometer-based gravimeters *Opt. Express* **26** 1586–96
- [32] Hensley J M, Peters A and Chu S 1999 Active low frequency vertical vibration isolation *Rev. Sci. Instrum.* **70** 2735–41
- [33] Peters A, Chung K Y and Chu S 1999 Measurement of gravitational acceleration by dropping atoms *Nature* **400** 849–52
- [34] Peters A, Chung K Y and Chu S 2001 High-precision gravity measurements using atom interferometry *Metrologia* **38** 25–61
- [35] Peterson J R 1993 Observations and modeling of seismic background noise *Open-File Report (New Mexico)*
- [36] Xue J and Shen B 2020 A novel swarm intelligence optimization approach: sparrow search algorithm *Syst. Sci. Control Eng.* **8** 22–34